Macromolecules

pubs.acs.org/Macromolecules Article

Unifying the Dynamics of Viscoelastic Liquids across the Complex Coacervation Phase Diagram: Time−Polyelectrolyte−Salt Superposition

Jialin She, Axel Bourdette Kaya, Jérôme Combet, Matthew Tirrell, Francisco J. Cedano-Serrano, Fouzia Boulmedais, and Mehdi Vahdati*

Cite This: *Macromolecules* 2026, 59, 1383−1396 Read Online

ACCESS | Metrics & More | Article Recommendations | Supporting Information

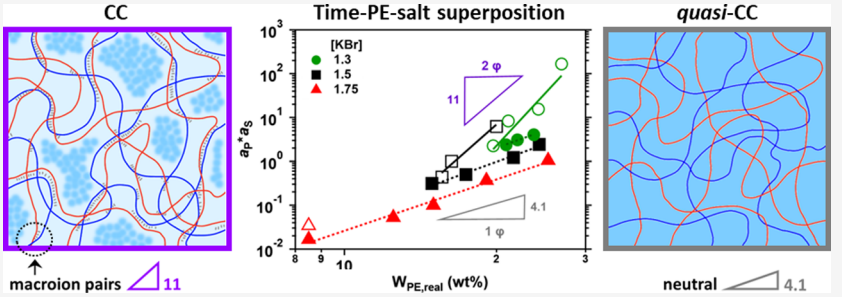

ABSTRACT: The dynamics and structure were investigated for polyelectrolyte-rich liquids across the high-salt region of the complex coacervation phase diagram of high molecular weight poly(4-styrenesulfonate), PSS, and poly(diallyldimethylammonium), PDADMA. The total concentration of polyelectrolytes (W_{PE}) was increased at different added KBr concentrations ([KBr]) to obtain liquid complex coacervates (CC) and single-phase, saline polyelectrolyte solutions. The dynamic response of these entangled polymer liquids was found to be self-similar at each [KBr], allowing a time−polyelectrolyte superposition using only a polyelectrolyte concentration-dependent horizontal shift factor, a_P. This self-similarity was further found among all the samples at different [KBr], allowing the construction of a universal master curve unifying the dynamics of all the samples by applying a second, salt-dependent horizontal shift factor, a_S. The CC dynamics were found to have a very strong dependence on the experimentally determined PE concentration with $a_P \propto W_{PE,real}^{11}$, while salty solutions of noninteracting PE behaved as polymers in good solvent with $a_P \propto W_{PE,real}^{4.1}$. The extreme scaling in the case of the CC defies the predictions for entangled associating polymers, probably due the large number of stickers per chain. Despite the absence of effective stickers in the salty solutions of fully doped polyelectrolytes, they can mimic the viscoelastic response of the CC up to the solubility limit of the PE. We called these materials *quasi*-complex coacervates (*quasi*-CC) to distinguish them from both CC and individual-polyelectrolyte solutions. Small-angle X-ray scattering revealed that PSS/PDADMA CC, their *quasi*-CC, and a PSS solution at the same total polymer and salt concentration all have different nanostructures. Unifying the dynamics of viscoelastic liquids across the high-salt region of the phase diagram, time−PE−salt superposition extends the classical time−salt and time−temperature superposition principles to PE systems, marking a step forward in understanding associative polymer dynamics.

INTRODUCTION

Complex coacervates (CC) are formed through the associative phase separation of oppositely charged polyelectrolytes (PE) into a polymer-rich phase in coexistence with a dilute phase.[1,2] The polymer-rich CC phase has widely tunable compositions and mechanical properties, all the way from stiff solids to water-rich low-viscosity liquids.[3,4] The association of the PE is reversible, for example, by adding high concentrations of salt. This aspect makes CC attractive in terms of properties such as self-assembly, reconfigurability, and recyclability. Therefore, physically cross-linked CC-based materials are emerging as promising alternatives to chemically cross-linked polymer networks in various application domains and have been the focus of extensive research and development in health,[5,6] energy,[7,8] and construction.[9,10]

The spontaneous association of the two PE is due to the attractive electrostatic interactions among their so-called macro-ions, driven by entropic gains from the release of the counterions and the restructuring of solvating water mole-

Received: September 29, 2025
Revised: December 23, 2026
Accepted: January 13, 2026
Published: January 23, 2026

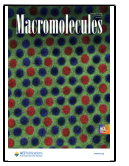

Scheme 1. (a) Schematic Phase Diagram with Negatively Tilted Tie Lines: The Samples Prepared at Initial [PE] and [KBr] (Point 0) Spontaneously Phase Separate into SN and CC Phases; (b) Different Pathways toward the Single-Phase Region of the Phase Diagram[a]

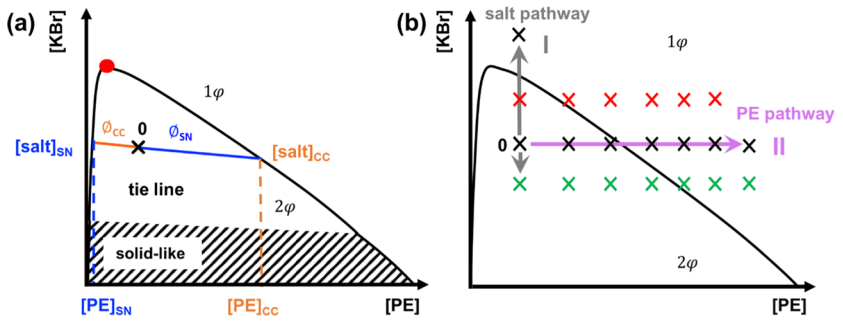

[a]A typical salt pathway (increasing [KBr] at a fixed [PE]), and a typical PE pathway (increasing [PE] at a fixed [KBr]) are schematized.

cules.[11,12] The formation of CC via phase separation is accompanied by the inevitable formation of a dilute, polymer-poor supernatant (SN).[13,14] The typically large volume of the SN favors the release of the counterions from the CC. The volume fraction of the coexisting phases is determined by the total salt and polymer concentrations as well as the affinity of the macro-ion pairs for one another. The salt−polymer plane of the phase diagram (Scheme 1a) offers a wealth of information about the complex coacervation behavior of a pair of PE. Such phase diagrams are usually experimentally determined by plotting the compositions of the coexisting phases at increasing salt concentrations until the point where the phase separation is suppressed.[4,15,16] The two-phase and the single-phase regions of the phase diagram are separated by the binodal curve, marking the *salt resistance* of the systems. Due to the associative nature of the phase separation, the binodal is highly asymmetrical with respect to the polymer concentration, with the critical salt concentration occurring close to the maximum salt resistance, typically at relatively low PE concentrations.[17−19]

The corresponding CC and SN compositions are linked via the tie lines, the slope of which is closely linked to the affinity of the macro-ions for one another.[17] The partitioning behavior of the PE with respect to their total concentration provides a rapid and reliable means of estimating the volume fraction of the coexisting phases (ϕ_{CC} and ϕ_{SN}). Known as the lever rule, this simple approximation is described by the following equations.

$$\phi_{CC} = \frac{V_{CC}}{V_{tot}} = \frac{[PE] - [PE]_{SN}}{[PE]_{CC} - [PE]_{SN}} \quad (1)$$

$$\phi_{SN} = \frac{V_{SN}}{V_{tot}} = \frac{[PE]_{CC} - [PE]}{[PE]_{CC} - [PE]_{SN}} \quad (2)$$

[PE], $[PE]_{CC}$, and $[PE]_{SN}$ are the molar concentrations of monomers in the total volume of the sample, in the CC, and in the SN, respectively. For convenience, we will use W_{PE} to note the total concentration of PE and $W_{PE,real}$ to refer to the experimentally determined concentration of the PE in the CC, both in wt %.

These basic but important insights about the phase behavior of oppositely charged PE can be used to establish relationships between the volume fraction, composition, and mechanical properties of the polymer materials obtained. As mentioned above, the effect of the added [salt] at a fixed W_{PE} has been studied in several insightful works.[4,5,20−22] The added (salt) ions "dope" or dissociate an increasing fraction of the macro-ion pairs between the PE, allowing more water molecules to enter the CC phase, causing it to swell.[20] This effectively increases ϕ_{CC} and decreases $[PE]_{CC}$. At high concentrations of a sufficiently chaotropic salt, the salt resistance of the system (the binodal) is exceeded, producing single-phase salty solutions of the two PE.[18,19]

The macro-ion pairs can be seen as transient cross-links or stickers with a lifetime $\tau_s = \tau_0 \exp\left(\frac{E_a}{kT}\right)$, where τ_0 is the characteristic time for thermal motion, E_a is the activation energy characteristic of the affinity of the sticker, and kT is thermal energy.[23,24] The sticker lifetime controls the relaxation dynamics of the chain on all longer time scales.[25,26] The dynamics of unentangled and entangled CC have been described using the sticky Rouse and sticky reptation models, respectively.[25,26] In either case, adding salt decreases τ_s, modifying all the longer relaxation times in a self-similar manner, allowing a so-called time−salt superposition.[27]

Most reported investigations of the dynamics of CC have considered the effect of changes in the polymer concentration of the CC phase to be negligible based on two assumptions. Some reports have assumed the salt-induced change in the polymer concentration to be small while others have argued that the theory of associative polymers predicts a small (on the order of unity) power-law dependence of the dynamics on the polymer concentration.[24,26,28] Both of these assumptions are questionable. The polymer concentration changes quite significantly by changing the salt concentration, as shown in several works.[4,13,14,26] Moreover, the theory of associative polymers predicts different scaling behaviors, ranging from 1.1 to 8.5, depending on the presence or absence of entanglements, the solvent quality, and the polymer concentration regime.[29] Several authors have pointed out that the dynamics of CC have a very strong dependence on the CC's polymer concentration. Still, a comprehensive understanding of the dependence of the dynamics on the polymer and salt concentration across the complex coacervation phase diagram is missing.[4,30−33] In fact, unlike the effect of changing the added salt concentration at a constant total concentration of PE (W_{PE}), the effect of changing W_{PE} (at a fixed added salt concentration) has been little studied, leaving large areas of the phase diagram uncharted, even for well-studied model systems.

In theory, the binodal boundary can also be crossed at a constant added salt concentration, leading to the so-called *self-suppression* of the complex coacervation. Such an observation

https://doi.org/10.1021/acs.macromol.5c02702
Macromolecules 2026, 59, 1383−1396

was first reported in the 1960s in a study of the complexation of charged biopolymers by Veis and colleagues.[34] Similar observations were reported in other systems.[14,35] In practice, this is only possible with PE that are sufficiently soluble to be mixed into a homogeneous solution outside the binodal boundary.[36] In analogy with the salt resistance, the self-suppression concentration (i.e., the binodal) can be regarded as the *polymer resistance* of the system. The self-suppression of the phase separation has (at least) two reasons. Despite the constant concentration of the *added* salt, an increase in W_{PE} is inevitably accompanied by a proportional increase in the counterion concentration. This effective increase in the *total* salt concentration has nontrivial consequences for the complexation behavior of the PE and the composition of the two phases, as elucidated in the work of Li and colleagues.[14] Moreover, the volume fraction of the SN phase decreases at higher W_{PE}, as predicted by the lever rule (eqs 1 and 2). Both of these factors make the release of the counterions less favorable and decrease the phase separation driving force.

To the best of our knowledge, no previous work has investigated the relationships between the composition and the dynamics of viscoelastic liquids obtained across the entire high-salt region of the phase diagram, i.e., both inside and outside the binodal boundary. Syed and Srivastava introduced a time−ionic strength superposition to describe the dynamics of semidilute unentangled CC prepared at different total polymer concentrations of fully charged poly(acrylic acid) and poly(allylamine) (PAA/PAH).[37] Their work highlighted the importance of taking into account the counterions added along with the PE on top of the added salt. In their analysis of the dynamics, the ionic strength shift factor ($a_I = a_S \cdot a_P$, taking into account all the small ions) had an exponential decrease as a function of the ionic strength within PAA/PAH CC. However, they did not examine how the dynamics depend on the real polymer concentration within the CC, nor did they investigate saline solutions of these polymers outside the two-phase region.[37] Laaser's group attempted to decouple the effects of the salt and polymer concentrations on the dynamics of CC via an original approach of directly adding salt into CC isolated from their SN.[31] They reported that the horizontal shift factor scales strongly with the polymer volume fraction, with exponents in the range of 3 to 6, much larger than the previous assumptions. However, the effect of the total PE in the two-phase region was not studied. Moreover, they prepared their samples in a particular way, which is different from the preparation methods used in the literature. Direct addition of dry salt to highly viscous CC does not ensure the homogeneity of the samples, an aspect which was not examined via scattering techniques.

The present work explores the composition, dynamics, and structure of viscoelastic liquids obtained across the entire high-salt region of the phase diagram for a model system based on high-molecular-weight poly(4-styrenesulfonate) and poly(diallyldimethylammonium) (PSS/PDADMA) doped with potassium bromide (KBr). The compositions of the CC, SN, and single-phase materials are carefully determined via thermogravimetric analysis, and an experimental phase diagram is constructed. Starting from an arbitrary reference formulation producing a liquid-like phase-separated CC (e.g., CC from point **0**, Scheme 1b), two types of pathways are explored toward different areas of the single-phase region of the phase diagram. A typical salt pathway corresponds to an increase in the added salt concentration, while a typical PE pathway corresponds to an increase in the PE concentration. The dynamics and structure of the PE-rich liquids obtained along different pathways are studied as a function of their salt and polymer contents. *Quasi*-complex coacervates (*quasi*-CC) are introduced as the single-phase (fully doped) samples that mimic the viscoelastic response of their phase-separated CC counterparts. While highlighting inherent differences between the CC and *quasi*-CC, a universal time−PE−salt superposition is proposed capturing the dynamics of all these materials in one universal master curve. We also show that the dynamics of *quasi*-CC are essentially different from those of saline solutions of PSS at the same total salt and polymer concentration. Finally, the structure of salty PSS solutions as well as the PSS/PDADMA CC and *quasi*-CC are studied.

MATERIALS AND METHODS

Materials

Poly(sodium 4-styrenesulfonate) (PSSNa) (M_w = 620 kg·mol^{-1}, M_w/M_n = 1.7) and poly(diallyldimethylammonium chloride) (PDADMAC) (M_w = 480 kg·mol^{-1}, M_w/M_n = 3.1), were purchased from Sigma-Aldrich and characterized by size exclusion chromatography. Potassium bromide (KBr, purity ≥ 99%) was also purchased from Sigma-Aldrich. The polymers and salt were used without further purification or modification. Milli-Q water (18.2 MΩ·cm resistivity at 25 °C) was obtained from a Q-POD purification system.

Sample Preparation

Individual stock solutions of PSSNa and PDADMAC at different polymer concentrations were prepared gravimetrically. A KBr stock solution was prepared at 4 M. All aqueous solutions were prepared using Milli-Q water. Briefly, given volumes of the stock solutions of PSS, KBr, and PDADMA were added in this order to a beaker under vigorous stirring. The SS/DADMA molar charge ratio was fixed at 0.85. The beaker was covered with Parafilm to avoid evaporation while maintaining the stirring for 3 h. Subsequently, the samples were transferred to 15 mL Falcon tubes and left to rest for 24 h. Finally, the samples were centrifugated for 30 min at 9000 rpm to clearly separate the two phases.

Total volumes ($V_{total} = V_{SN} + V_{CC}$) were directly read from the Falcon tubes. The SN phase was gently removed from the Falcon tube and its volume (V_{SN}) was calculated after measuring its mass and density. The volume of the CC phase (V_{CC}) was calculated by subtracting V_{SN} from V_{total}. The sample preparation and volume determination were conducted at room temperature. The typical error in our volume determination method is less than 4 vol %. The reported *total* (as prepared) concentrations of PE (in wt %) and [KBr] (in M = mol L^{-1}) are nominal and do not consider volume changes. The samples were stored in their Falcon tubes at 4 °C until further use. The samples were left at room temperature for at least 1 before all experiments. Before characterizations, the SN was then carefully removed from the Falcon tube.

Characterization Methods

Thermogravimetric Analysis (TGA). The TGA experiments were performed on a TGA2 large-furnace machine (Mettler Toledo) using aluminum oxide crucibles. All experiments were carried out under a constant air flow at 100 mL·min^{-1}. The samples were first subjected to a temperature ramp from 25 to 150 °C at a heating rate of 10 °C·min^{-1}, followed by an isotherm for 20 min. The samples were then heated to 1000 °C at a heating rate of 20 °C·min^{-1}. The water, polymer, and salt contents of the CC, their corresponding SN, and single-phase samples were calculated as detailed in Figure S1 in the Supporting Information. The water content was determined from the mass loss after the isotherm at 150 °C. The polymer content was calculated from the mass loss between 150 and 700 °C. The residue content is determined by the remaining mass at 700 °C, containing the residues from PE and added salt. To deconvolute the TGA data, reference curves of PSS and PDADMA with or without added salt as

https://doi.org/10.1021/acs.macromol.5c02702
Macromolecules 2026, 59, 1383−1396

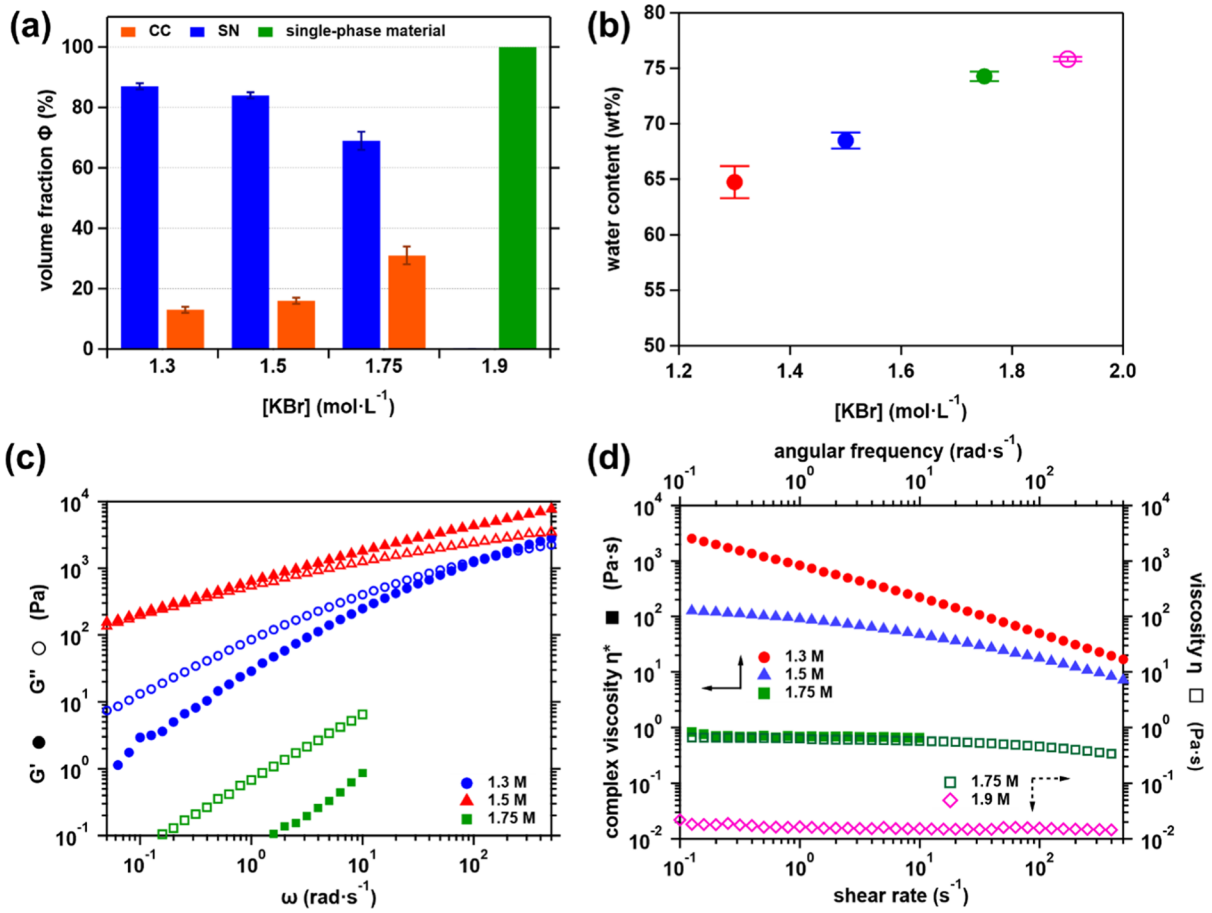

Figure 1. (a) Volume fraction of PSS/PDADMA CC and SN as a function of KBr concentration. (b) Water content of PSS/PDADMA CC as a function of KBr concentration. (c) Storage modulus (G', ●) and loss modulus (G'', ○) of PSS/PDADMA CC at different KBr concentrations. (d) Complex viscosity (η^*) of PSS/PDADMA CC at 1.3, 1.5, and 1.75 M KBr and viscosity (η) of PSS/PDADMA CC and salty solution at 1.75 and 1.9 M KBr, respectively.

well as those of NaCl and KBr were measured individually. It was determined that 59 wt % of PSS and 93 wt % of PDADMA were degraded between 150 and 700 °C, corresponding to 41 and 7 wt % of residues for PSS and PDADMA, respectively. The content of added salt was determined by extracting the residue ratios of PE from the total residue mass ratio. The typical error in our TGA measurements is less than 1.0 wt %.

(Underwater) Linear Rheology. In all experiments, a stress-controlled HR-20 rheometer (TA Instruments) equipped with an immersion cup and a Peltier temperature control system was used. All rheological measurements were performed at 20 °C under a vapor trap to minimize evaporation. In the case of the phase-separated samples, each CC was studied while immersed in its SN. A sandblasted plate−plate geometry with a diameter of 20 mm and a gap height of 500 μm was used in the case of the highly viscoelastic samples. The more liquid-like samples were tested using a cone−plate geometry with a cone angle of 4° and a diameter of 40 mm. Oscillatory amplitude sweeps were performed from 0.01 to 10% strain to determine the limit of the linear regime. The samples were then tested in frequency sweeps from 0.05 to 500 rad·s^{-1} at a fixed strain within the linear regime (≤0.5% depending on the sample). All the superpositions were performed after verifying the feasibility based on Cole−Cole plots.

Rotational Rheology. The flow behavior of the low-viscosity samples was studied on the rheometer presented above. A 40 mm stainless cone−plate geometry with a cone angle of 1° was used to subject the samples to shear rates between 10^{-1} and 10^{3} s^{-1}. The tests were carried out at 20 °C under a solvent trap to minimize compositional changes due to evaporation.

Small Angle X-ray Scattering. Small angle X-ray scattering (SAXS) measurements were performed on the SWING beamline at the SOLEIL synchrotron (Saint-Aubin, France). The beam energy was set to 16 keV (wavelength λ = 0.78 Å). Two sample-to-detector distances were used, covering a scattering vector range between q = 0.002 and 2 Å^{-1} (with $q = \frac{4\pi \sin(\theta)}{\lambda}$, where 2θ is the scattering angle). Scattered intensities were recorded on an Eiger 4M detector (Dectris Ltd., Switzerland, pixel size 75 × 75 μm^2). Data reduction was carried out following standard procedures for isotropic scattering. Intensities were scaled to absolute units using a Lupolen standard. Each sample was measured in borosilicate capillaries (1.6 mm diameter) at room temperature (20 °C), with an exposure time of 2 s. Final data were corrected for capillary, solvent, and KBr contributions, yielding the scattering cross-section of polymers per unit volume of solution, $I(q)$ (cm^{-1}).

RESULTS AND DISCUSSION

A Typical Salt Pathway: Changing [KBr] at Constant [PE]

The evolution of the phase behavior and the viscoelastic properties of the CC were studied along a typical salt pathway (Figure 1). Samples were prepared at 1.3, 1.5, 1.75, and 1.9 M KBr at a fixed total W_{PE} of 4.6 wt % ([PE] = 0.28 M). As [KBr] was increased from 1.3 to 1.75 M, the CC phase showed a nonlinear increase in the volume fraction and water content, effectively reducing the $[PE]_{CC}$, as reported in previous works (Figure 1a,b).[13,19,22,25,31] The measured changes in the volume fraction of the two phases are in quantitative agreement with

https://doi.org/10.1021/acs.macromol.5c02702
Macromolecules 2026, 59, 1383−1396

our predictions based on the lever rule (eqs 1 and 2, Table S1 in Supporting Information).

At 1.9 M KBr, all the macro-ion pairs were dissociated by KBr, and the phase separation was suppressed.[38] The phase diagram corresponding to the samples prepared at W_{PE} = 4.6 wt % with increasing [KBr] is presented in Figure S2 in the Supporting Information. The tie lines are negatively sloped, showing that the complexation of PSS and PDADMA is exothermic, with KBr preferentially partitioning in the SN phase. This is in qualitative agreement with the work of Liu and colleagues, who found steeper negative slopes and slightly lower polymer concentrations in the CC.[4] The difference in [KBr] in the CC and SN becomes less significant at higher salt concentrations, flattening the tie lines toward the critical point where the excluded volume effects become less important.[12,14] The reduced excluded volume effects and the larger water contents lower the entropic gain from counterion release and water reorganization, leading to the suppression of the phase separation.

The viscoelastic behavior of these materials was quantified using frequency sweeps and shear viscosity measurements (Figure 1c,d). At 1.3 M KBr, the CC is a highly viscoelastic material close to the critical gel point. In comparison, the samples at 1.5 and 1.75 M KBr have the characteristic behavior of semidilute polymer solutions. The longest relaxation time of the system (τ_c), corresponding to the inverse of the crossover frequency ($\tau_c = \frac{1}{\omega_c}$), decreased by nearly 3 orders of magnitude when [KBr] was increased from 1.3 to 1.5 M. This crossover was not within the measurable range of frequency at higher salt concentrations. This suggests that only the samples at 1.3 and 1.5 M are in the *entangled* regime. In the case of the 1.75 M CC, a relative viscosity ($\eta_r = \frac{\eta_0}{\eta_s}$, with η_s the solvent viscosity) of 660 may seem to suggest that this CC is also in the semidilute *entangled* regime.[39] However, the absence of a terminal relaxation time (crossover in G' and G'') in its linear viscoelastic response clearly indicates that this CC is still in the semidilute *unentangled* regime (Figure 1c). Such a discrepancy has been discussed in recent works on the occurrence of entanglements in PE solutions,[40,41] which have shown that using the above-mentioned viscosity-based criterion underestimates the crossover to the entangled regime in PE solutions. Likewise, the single-phase liquid obtained at 1.9 M KBr with a relative viscosity of 15 is in the semidilute *unentangled* regime.[19,39] These results highlight the significant acceleration of the dynamics of CC as a result of the addition of salt, which is known to reduce the lifetime and the effective density of the macro-ion pairs and to decrease the polymer volume fraction.[4,24,26,38] The effective absence of the macro-ion pairs above the salt resistance takes the system back to the case of a neutral polymer solution with no stickers to slow the dynamics.

In summary, following a salt pathway toward the single-phase region results in much lower $W_{PE,real}$ and significantly accelerated dynamics, especially at the point where the binodal boundary is crossed. The effect of the added salt is particularly more pronounced below the entanglement monomer concentration.

Typical PE Pathways: Changing [PE] at Constant [KBr]

The effects of W_{PE} on the phase behavior and dynamics of PE CC are little understood. We prepared three series of PSS/PDADMA formulations along typical PE pathways at 1.3, 1.5, and 1.75 M KBr. For each series (i.e., each [KBr]), the PE concentration was varied between 4.6 wt % ([PE] = 0.28 M, point **0**) and 25.2 wt % ([PE] = 1.64 M), which is the solubility limit of these PE under the conditions of the present study. We start by presenting a typical PE pathway at 1.5 M KBr before discussing the other PE pathways at 1.3 and 1.75 M KBr. The increase in W_{PE} toward the binodal boundary results in a monotonic increase in the volume fraction of the CC (Figures 2a and S3 in the Supporting Information). The experimentally determined volume fractions of the two phases, ϕ_{CC} and ϕ_{SN}, are in agreement with the prediction of the lever rule (Table S2 in the Supporting Information), indicating that these samples are not far from equilibrium. At 1.5 M KBr, the

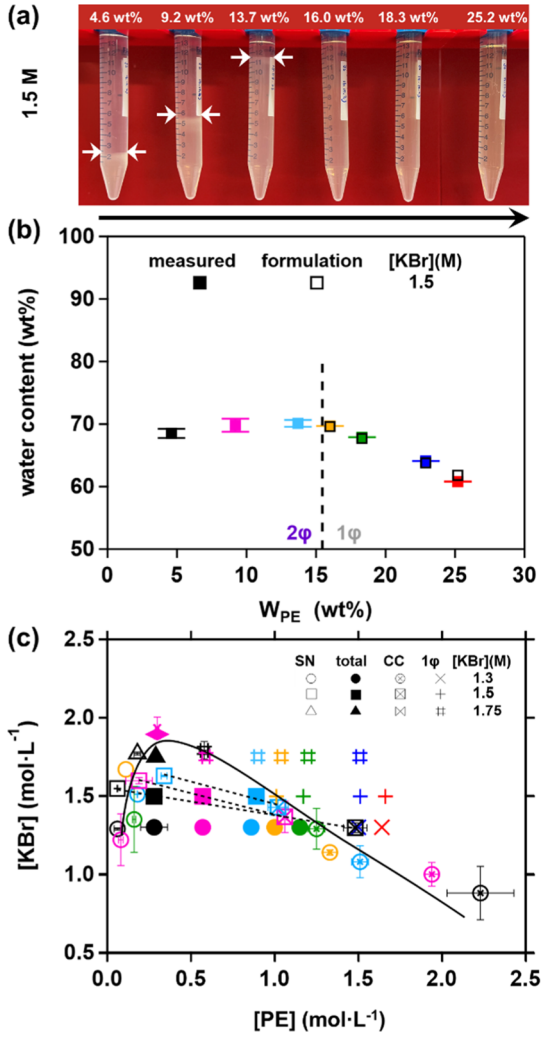

Figure 2. (a) Photos of PSS/PDADMA formulations prepared at different W_{PE} at 1.5 M KBr. The arrows indicate the boundary between the CC (bottom) and SN (top) phases in the phase-separated samples. (b) The water content of the polymer-rich materials, determined by TGA (full circles). In the case of the single-phase samples, the experimental values are compared to those from the formulation (hollow black squares). (c) The experimental phase diagram of PSS/PDADMA formulations at different KBr concentrations. The binodal boundary (solid black line) is a visual guide. The tie lines (only shown for the sample at 1.5 M KBr) are represented by the black dashed lines. The data from the samples at 1.3 and 1.75 M can be found in the Supporting Information (Figure S3f,g in the Supporting Information).

https://doi.org/10.1021/acs.macromol.5c02702
Macromolecules 2026, 59, 1383−1396

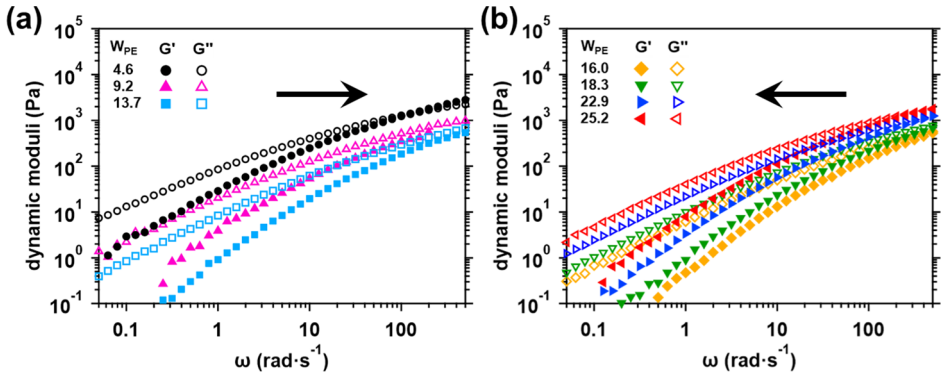

Figure 3. Rheological behavior, storage (G') and loss (G'') modulus, of the PSS/PDADMA (a) phase-separated CC and (b) single-phase materials prepared at different W_{PE} at 1.5 M KBr. Arrows indicate the shift in dynamics as a function of the total concentration of PE.

phase separation is self-suppressed somewhere between 13.7 and 16 wt % PE.

Figure 2b presents the water content of the polymer-rich materials at different W_{PE}. The trend in the water content was found to reverse when crossing the binodal boundary (Figure 2b). The polymer-rich phase slightly swelled toward the binodal boundary, but in the absence of phase separation, the water content decreased monotonically as more PE was added. Generically similar trends were found at 1.3 and 1.75 M KBr where liquid-like CC are obtained, see Figure S3d,e in the Supporting Information. This is not surprising given the arbitrary choice of point **0**. We note that the PE pathways at higher salt concentrations have larger ϕ_{CC} and water contents at comparable W_{PE}, implying the reduced entropic gain from reduced excluded volume effects at larger water content. As such, the W_{PE}, where complex coacervation is self-suppressed, decreases at higher added KBr. The experimentally determined phase diagram in Figure 2c shows the concentrations of PE and KBr for the samples prepared along the PE pathway at 1.3, 1.5, 1.75, and 1.9 M KBr.

To understand the trends described above, one must consider that following a PE pathway corresponds to a proportional increase in the concentration of the counterions. As discussed in the works of Li et al. as well as Syed and Srivastava, the addition of PE reduces the available volume for counterion release, effectively swelling the CC phase.[14,37] This reduces the entropic gain of counterion release and slightly decreases the enthalpic change as the water molecules are less disordered in comparison to pure water.[12,14,42] Meanwhile, the added counterions effectively increase the total *salt* concentration. Therefore, the total driving force for coacervation decreases with increased W_{PE} toward the binodal boundary, where the phase separation is self-suppressed (Figures 2 and S3 in the Supporting Information). Importantly, the swelling is less pronounced along the PE pathway (2−3 wt % additional water, Figure 2b) when compared to the salt pathway (10−11 wt % additional water, Figure 1b). This suggests that adding salt is more effective than adding PE in suppressing complex coacervation.

Next, we investigated the linear viscoelastic properties of the polymer-rich materials obtained at increasing W_{PE} at 1.5 M KBr (Figure 3a,b). All the samples show the characteristic viscoelastic behavior of semidilute polymer solutions with a crossover in the storage modulus and loss modulus ($G' = G''$) and the appearance of the low-frequency end of the rubbery plateau.

The inverse of the crossover frequency corresponds to the longest relaxation time, i.e., the reptation time (τ_{rep}), which is the time for a chain to diffuse out of the entanglement tube. As W_{PE} is increased toward the binodal boundary, the crossover of the phase-separated CC shifts to higher frequencies (shorter τ_{rep}, Figures 2b,c and 3a), indicating accelerated dynamics and enhanced chain mobility. The increasingly liquid-like behavior of the CC prepared at higher W_{PE} is consistent with (i) the increased charge screening as the *total* salt concentration goes up and (ii) the lower polymer volume fractions in the CC due to the negative slope of the tie lines.

Beyond the phase boundary, the viscoelastic profile remains similar but τ_{rep} slightly increases with W_{PE} (Figure 3b). This is in agreement with the changes in the composition (Figure 2b,c). The dynamics of the single-phase materials obtained are determined by two competing effects. While the added polymer volume fraction slows the dynamics, the inevitably added counterions tend to accelerate the dynamics by decreasing the chain size.[39,43] The slowed dynamics of the single-phase samples suggests that the positive contribution of the added PE dominates the effect of their counterions. This is not surprising given that these salty PE solutions are moderately entangled.[40] The linear viscoelastic properties of the samples prepared at 1.3 and 1.75 M KBr show similar dynamic responses, with faster and slower dynamics as W_{PE} is increased inside and outside the binodal boundary, respectively (Figure S4 in the Supporting Information). While all the samples at 1.3 M are in the *semidilute entangled* regime, with the one at 4.6 wt % PE behaving as a critical gel (Figure S4a in the Supporting Information), all the samples at 1.75 M are *unentangled*, with the most concentrated sample (22.9 wt %) at the onset of entanglements (Figure S4d in the Supporting Information).

Time−PE Superposition: From Complex Coacervates to *Quasi*-Complex Coacervates

Along PE pathways, the trend in the dynamic response of the polymer-rich liquids was shown to reverse at the binodal boundary (Figures 3 and S4 in the Supporting Information). We found that the dynamic response of all the PE-rich liquids along a PE pathway is self-similar, regardless of whether they were obtained via phase separation or not. A Cole−Cole analysis was used to confirm the feasibility of a superposition along each PE pathway (Figure S5 in the Supporting Information; we note that the sample at 4.6 wt % PE and 1.3 M KBr was excluded from the superposition due to its critical gel behavior). At each salt concentration, only a

https://doi.org/10.1021/acs.macromol.5c02702
Macromolecules 2026, 59, 1383−1396

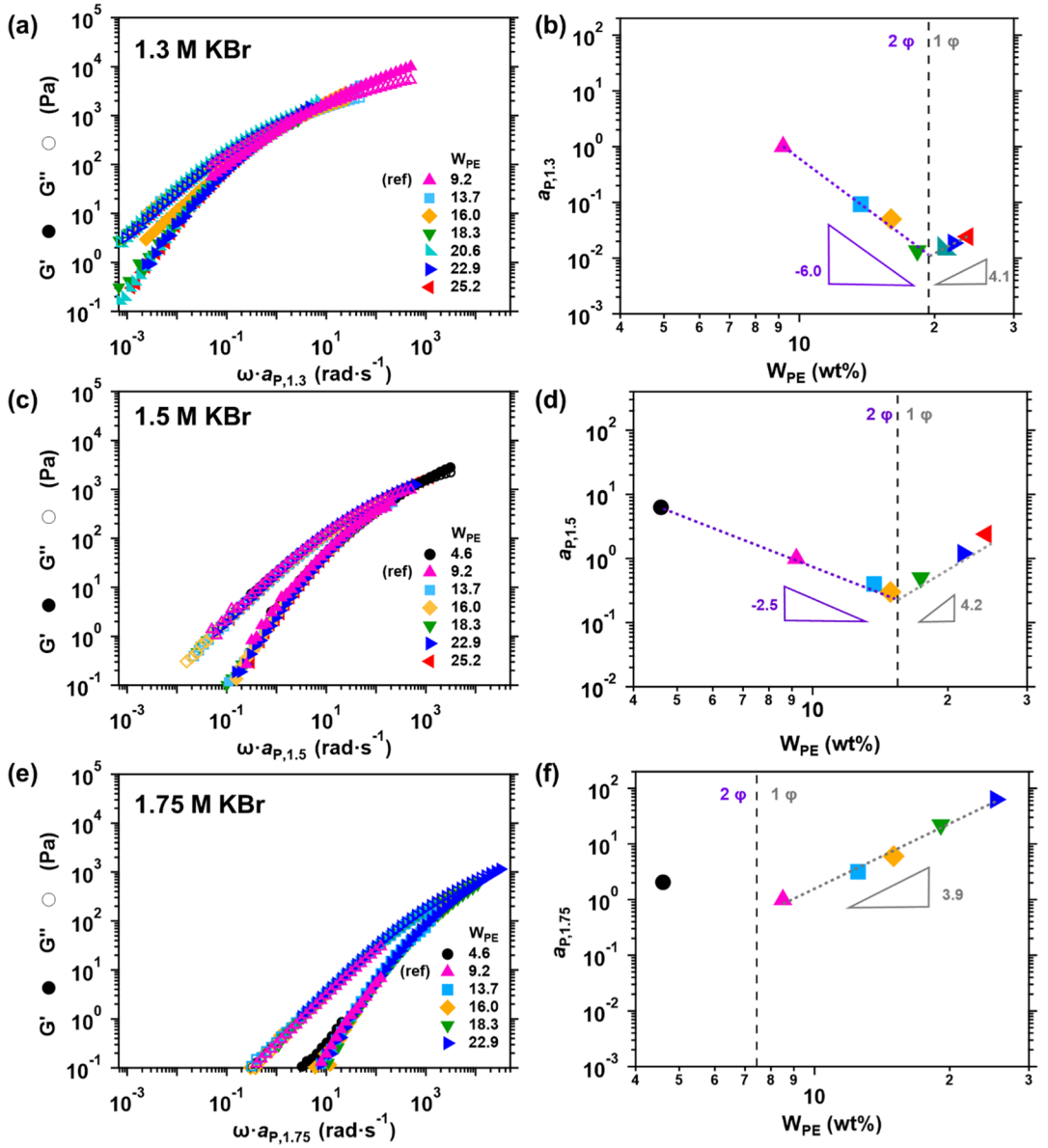

Figure 4. On the left panel, master curves obtained from time−PE superposition at samples prepared at (a) 1.3, (c) 1.5, and (e) 1.75 M with varying W_{PE}. The single-phase material obtained at 9.2 wt % PE at all prepared KBr concentrations was chosen as the reference (shift factor, a_P = 1), and the rheological data of the other samples were superimposed using an individual horizontal shift factor (a_P) relative to this reference. On the right panel, the relationship between a_P and total W_{PE} at (b) 1.3, (d) 1.5, and (f) 1.75 M KBr. The black dashed line represents the calculated binodal limit except for 1.75 M KBr. The uncertainty of the power-law exponent (β) presented is ±0.5.

horizontal shift factor, a_P, was used to shift the curves with respect to the single-phase sample obtained at 9.2 wt % PE as an arbitrary reference. It was verified that no vertical shift factor was needed, which is somewhat counterintuitive given the changes in the polymer fraction. The implications of this time−PE superposition, reported for the first time here, are manifold, as discussed in the following.

The left panel in Figure 4 presents the master curves obtained for the samples prepared at different W_{PE} at 1.3, 1.5, and 1.75 M KBr, respectively. The master curve at 1.3 M KBr is admittedly less perfect than the ones at higher [KBr], with the appearance of slower modes at lower polymer concentrations due to the proximity of these samples to the gel point. Nevertheless, the addition of salt clearly promotes faster dynamics, as seen in the decrease of the observable τ_{rep} of the samples prepared at 1.3 and 1.5 M KBr ($\tau_{rep,1.3}$ = 200 ms and $\tau_{rep,1.5}$ = 1 ms). At 1.75 M KBr, the crossover of the dynamic moduli is barely accessible, with an estimated τ_{rep} around 0.03 ms.

A significant insight from the superposition is that the fastest dynamics, or the lowest zero-shear viscosity, along each PE pathway, corresponds to the sample prepared at the binodal boundary. This is seen in the plots of a_P as a function of the total concentration of PE (right panel Figure 4). We found power-law dependencies of the form $a_P \propto W_{PE}^{\beta}$ with different β exponents inside and outside the binodal boundary. In the two-phase region, exponents of −6.0 and −2.5 were found for the pathways at 1.3 M KBr and 1.5 M KBr, respectively. The larger negative exponent at 1.3 M indicates that the viscoelastic properties of the CC obtained at a lower salt concentration, where coacervation is more favorable, have a stronger dependence on the total W_{PE}. In the single-phase region, the

https://doi.org/10.1021/acs.macromol.5c02702
Macromolecules 2026, 59, 1383−1396

samples prepared at 1.3, 1.5, and 1.75 M added KBr show a power-law scaling with β = 4.1, 4.2, and 3.9, respectively. The fact that all these samples have similar exponents is not surprising, given that they are all practically salty, concentrated solutions of the same two PE with no macro-ion pairs acting as stickers. The scaling predictions for entangled solutions of neutral polymers in good solvent and θ solvent conditions are 3.9 and 4.7, respectively.[39] An exponent of around 4.1 for the single-phase samples reasonably suggests rather good solvent conditions.[39,44]

These scaling laws from viscoelastic measurements can be used to predict the binodal boundary along each PE pathway. The intersections of the two power laws at 19.4 and 15.2 wt % PE are in excellent agreement with the experimental polymer concentration where the phase separation is self-suppressed at 1.3 and 1.5 M KBr, respectively (Figures 2 and S4 in the Supporting Information). In other words, here we have exploited simple viscoelastic analyses to obtain information about the phase behavior of mixtures of oppositely charged PE. This is broadly comparable to the analysis in the seminal work of Wang and Schlenoff, where the authors distinguished PSS/PDADMA CC from their saline solutions based on an abrupt change in the salt-dependent slope of the complex viscosity, that is, along a salt pathway in our terms.[22] We note that their investigation was limited to a single frequency rather than considering the whole viscoelastic response of the materials studied.

As discussed above, the correlation of a_P with the W_{PE} reflects the thermodynamic favorability of coacervation and enables the prediction of the binodal boundary. Nonetheless, in the case of the phase-separated samples, the real polymer concentration in the CC phase is actually much higher than the total W_{PE} (except when the samples are prepared close to the critical point or close to the binodal boundary). Therefore, the horizontal shift factor, a_P, was plotted as a function of the real polymer concentration ($W_{PE,real}$) in Figure 5a–c. Surprisingly, power law fits to the data for the phase separated samples show similar and extremely large exponents of β = 12.4 and β = 10.2 for the samples prepared at 1.3 and 1.5 M KBr, respectively. These surprising exponents are admittedly obtained from power law fits over a rather narrow range of real polymer concentrations limited by the phase separation process (which is why we consider β = 12.4 and β = 10.2 to have a similar significance). Nevertheless, they clearly point to a significant dependence of the dynamics of CC on the real polymer concentration.

The polymer concentration dependence has remained largely overlooked despite several mentions in the literature. Liu and colleagues briefly pointed that the time–salt superposition shift factor has a very strong correlation with the CC's polymer concentration.[4] Perry and Schiffman found that the zero-shear viscosity scaled with $W_{PE,real}^{\beta}$ with β varying between 7 and 10.5 for entangled CC from poly(3-sulfopropyl methacrylate potassium salt) (PSPMA) and poly([2-(methacryloyloxy)ethyl]trimethylammonium iodide) (PTMAEMA).[32] However, they did not explore these results any further. More recently, Landfield and Wang clearly showed that the dynamics of PE solutions and mixtures are extremely strongly dependent on the polymer concentration in highly crowded environments.[33,45] They reported that the tracer diffusivity (inversely proportional to the viscosity) decreased with the polymer concentration to the power −6.1 to −6.5 in the case of both solutions and CC, while microrheology and

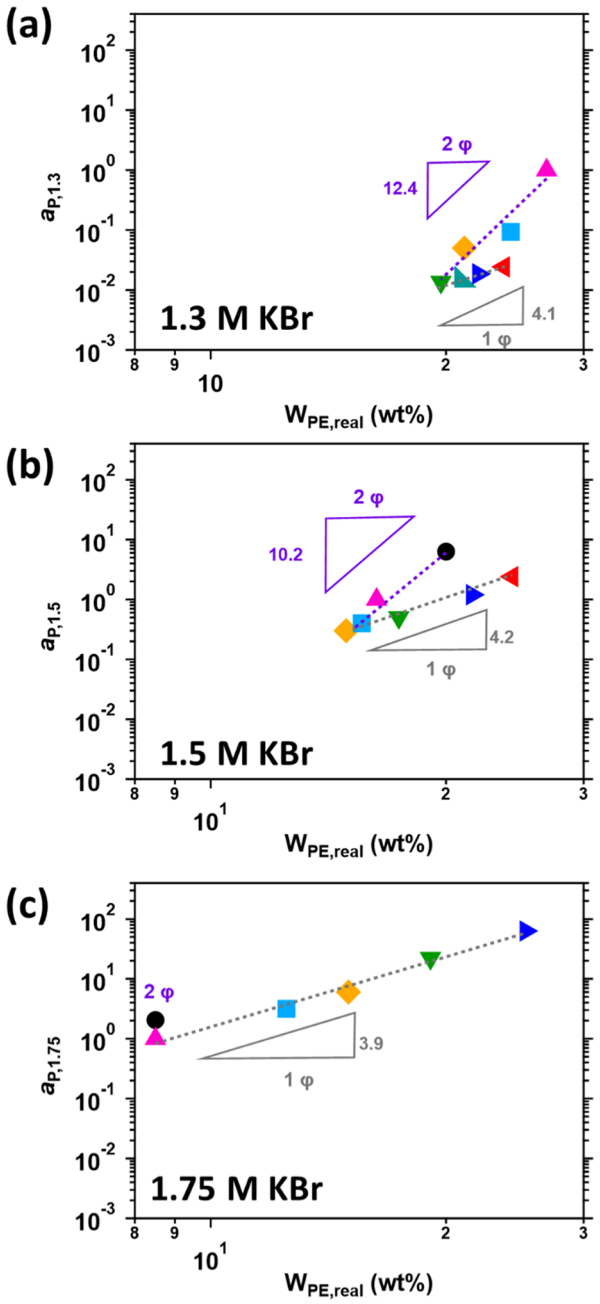

Figure 5. Relationship between a_P and real PE concentration, $W_{PE,real}$, at (a) 1.3 M, (b) 1.5 M, and (c) 1.75 M KBr. The purple and cyan dashed lines refer to power-law fits of a_P as a function of W_{PE} in the two-phase region and the single-phase region, respectively. The uncertainty in the power-law exponent β for the phase separated and single-phase samples was determined to be ±1.5, and ±0.5, respectively.

bulk rheology experiments showed that the viscosity of highly concentrated polylysine solutions scaled with $W_{PE}^{7.2\pm4.0}$. The authors suggested that the extremely slow dynamics at high polymer contents are due to the establishment of glassy dynamics due to the large excluded volume of the charged species at low water contents. The group of Laaser reported time–salt superposition horizontal shift factors scaling with $W_{PE,real}^{\beta}$ with β in the range of 3–6 in a PSS/PDADMA system with extra KBr added to the CC after isolation from the SN.[31] Most of their samples were effectively in the single-phase

https://doi.org/10.1021/acs.macromol.5c02702
Macromolecules 2026, 59, 1383–1396

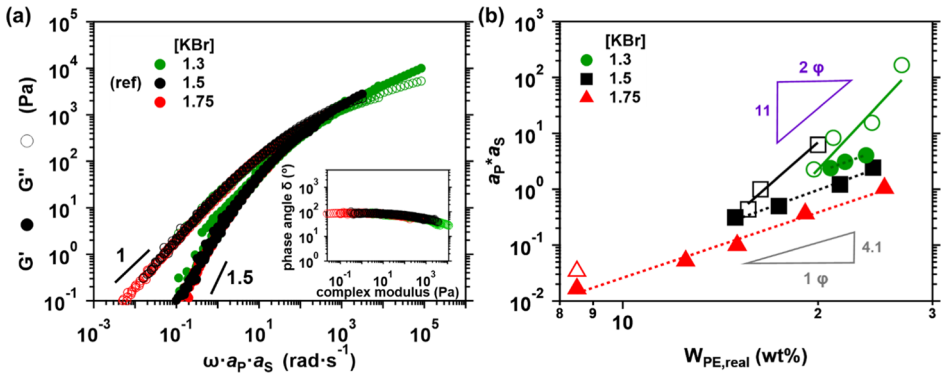

Figure 6. (a) The master curves of master curves obtained at different KBr concentrations with increasing W_{PE}. To construct the universal master curves including formulations at different salt and polymer concentrations, a second horizontal shift factor related to the salt concentration (a_S) was applied to the time−PE master curves (Figure 4). Samples at 1.5 M are chosen as the reference ($a_P \cdot a_S = 1$). The inset depicts the Van Gurp−Palmen plot used to verify the feasibility of the superposition. (b) The shift factor, $a_P \cdot a_S$, as a function of the real W_{PE} in the polymer-rich phase. The solid and dashed lines are the power law fits for the two-phase and single-phase samples, respectively.

region, which could explain the smaller exponents found compared to those of the CC in our study. We believe that the different exponents in the literature arise from differences in (i) the affinities of different charged groups for one another, (ii) concentration regimes, and (iii) the preparation methods. Our samples were all prepared in the same way at different W_{PE} and were within or very close to the semidilute entangled regime.

While the exponent of the single-phase region (β = 4.1) in Figure 5 may be understood based on the scaling theory, the very large exponents for the two-phase samples in our work and those of others defy the predictions of the scaling theory of entangled associative polymers, which predicts exponents as large as 6.8 as the concentration is increased above the entanglement concentration.[29,39] We believe that the presence of charges on oppositely charged PE, the presence of large quantities of small ions in these liquid-like systems, and the large number of stickers per chain complicate the direct application of the aforementioned theories to the case of CC. To begin with, an important assumption in the theory proposed by Rubinstein and Semenov is the sparsity of the stickers (many noninteracting monomers between stickers), which is not the case for CC at most compositions.[29] This theory also does not take electrostatic effects, such as charge−charge interactions into account. Our results call for more adapted theoretical frameworks for the dynamics of CC. For instance, the sticky-blob model developed by Parisi and co-workers describes the dynamics of entangled solutions of a single polymer with many stickers per correlation blob in athermal and θ solvent conditions.[46] With a few modifications to consider the specificities of PSS/PDADMA CC, the sticky-blob model may be well-suited to capturing the dynamics of our system and other complex coacervates.

The last (but not the least) insight from the time−PE superposition (Figures 4 and 5) is that the single-phase samples; i.e. saline solutions of PE, mimic the viscoelastic response of liquid-like CC *without* phase separation. Given that the samples with the same a_P have the same dynamic response, we find that the samples prepared outside the binodal region are, in fact, the single-phase viscoelastic analogs of the CC obtained via phase separation. We have called these materials *quasi*-complex coacervates (*quasi*-CC) to distinguish them from both CC and individual-PE solutions (as discussed later). A *quasi*-CC is thus a saline solution of fully doped (i.e. noninteracting) oppositely charged PE with the same linear viscoelastic behavior as a reference phase-separated CC. For example, the sample prepared at 22.9 wt % PE and 1.5 M KBr is the *quasi*-CC of the CC obtained at 9.2 wt % PE and 1.5 M KBr.

We note that at a given [KBr], the limited solubility of our moderately hydrophilic PE places an upper limit on the viscosities that can be attained without associative phase separation. As an example, at 1.5 M KBr, the PSS/PDADMA system reaches the polymer solubility limit at around 25 wt %; however, replicating the viscoelastic response of the CC at 4.6 wt % PE is predicted (based on the power law behavior shown in Figure 4d) to require a practically unattainable polymer concentration of 31.7 wt %. This means that merely increasing the polymer concentration to attain the equivalent level of entanglements in a *quasi*-CC is not always sufficient to mimic the dynamic response of a CC, which is further slowed down by the macro-ion stickers on top of the existing entanglements.

Via time−PE superposition, the effects of W_{PE} and $W_{PE,real}$ were systematically investigated for the first time. Notably, the $W_{PE,real}$ is clearly not a negligible factor in the dynamics of CC. In the high-salt region of the phase diagram, the addition of W_{PE} is analogous to the effects of adding salt before the coacervation is (*self*)-suppressed. The increase in W_{PE} accelerates the dynamics of the obtained CC with the fastest dynamics at the binodal boundary. A strong power-law correlation $a_P \propto W_{PE,real}^{11\pm1.5}$ is observed. Whether this relationship is specific to certain polymer systems remains an open question and requires further investigation. Herein, time−PE superposition is proposed as a further extension of the superposition family applied to study the effects of polymer concentration on the dynamics of CC.

Time−PE−Salt Superposition: Unifying the Dynamics across the Phase Diagram

We further found that the master curves at different [KBr] are also superimposable as verified by Cole−Cole plots (Figure S6 in the Supporting Information) and Van Gurp−Palmen (inset in Figure 6a), allowing to build a universal master curve for all the PE-rich liquids obtained at various [KBr] and W_{PE}. As was done in the case of time−PE superposition, a second horizontal shift factor, a_S, now a function of the added KBr concentration, was applied to superimpose the individual master curves (on the left panel, Figure 4) onto the universal master curve with 9.2 wt % PE and 1.5 M KBr as the reference

https://doi.org/10.1021/acs.macromol.5c02702
Macromolecules 2026, 59, 1383−1396

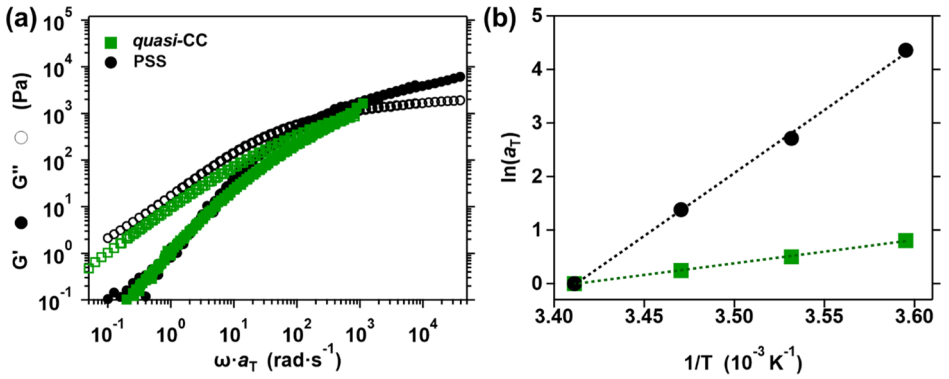

Figure 7. (a) Time−temperature superposition master curves and (b) the temperature dependence of the shift factor, a_T, and temperature of *quasi*-CC and its equivalent PSS solution.

(Figure 6a). This master curve clearly shows a viscoelastic liquid-like behavior revealing the onset of a rubbery plateau. The reptation time, τ_{rep}, from the crossover of G' and G'' is around 1 ms, comparable to that of the entangled poly(methacrylic acid) (PMAA) and poly[3-(methacryloylamino)propyltrimethylammonium chloride] (PMAPTAC) CC obtained at high-molecular-weight and low salt concentration ([NaCl] = 0.3 M).[26] At very low frequencies, G'' shows the expected ω^1 scaling but $G' \propto \omega^{1.5}$, which is smaller than the expected scaling of $G' \propto \omega^2$ for polymer solutions and melts.[47] This implies a delayed relaxation behavior and the presence of multiple relaxation modes possibly due to the large polydispersity of the polymers used in this work, in agreement with the results of Ali and Prabhu and Liu et al.[4,30]

More importantly, this universal superposition indicates that all the liquid-like samples across the phase diagram have self-similar dynamics, regardless of the occurrence or absence of phase separation. Nevertheless, the dynamics of the CC and *quasi*-CC (single-phase saline solutions of noninteracting PE) are controlled by different mechanisms. The terminal relaxation time is a *sticky* reptation time for the CC and a *simple* reptation time in the case of the saline PE solutions. In both entangled cases, this is the characteristic time for a chain to emerge from the entanglement tube.[29] In the case of the CC, this time is slowed down by the stickers along the tube when compared to a solution of noninteracting polymers. As in other associating systems, the dynamics of CC are slowed down by τ_s/τ_0.[25,26,29,47] In the case of the *quasi*-CC, an exponent of ∼4.1 suggests that there are no net electrostatic interactions among the two PE, implying that the relaxation time is the simple reptation time of neutral polymer chains.

The different mechanisms controlling the dynamics of CC and *quasi*-CC clearly manifest themselves in the total shift factor, $a_P \cdot a_S$, as a function of the real polymer concentration, $W_{PE,real}$, as shown in Figure 6b. The dependence of $a_P \cdot a_S$ on W_{PE} is presented in Figure S7 in the Supporting Information. Figure 6b shows that the dynamics of all the CC are controlled by the same sticky reptation mechanism, as seen by $W^{\beta}_{PE,real}$ with β around 11 at different salt and polymer concentrations. Likewise, the dynamics of all the *quasi*-CC can be described by the same reptation mechanism, leading to a similar of $W^{\beta}_{PE,real}$, with β around 4.1 at different salt and polymer concentrations in the single-phase region. Based on these universal observations, we propose that the plots in Figures 6b and S7 in the Supporting Information may be considered as viscoelastic phase diagrams or the viscoelastic fingerprint of these CC and *quasi*-CC.

Quasi-Complex Coacervates Versus Individual Polyelectrolyte Solutions

A *quasi*-CC is essentially a saline solution of two non-interacting PE, which makes it different not only from CC, as discussed above, but also from a saline solution of an individual PE. In this section, we compare the dynamic response of a *quasi*-CC with an equivalent PSS solution (Figure S8 in the Supporting Information) using frequency sweeps at different temperatures. The PSS solution was at 18.3 wt % PSS, while the *quasi*-CC was composed of 18.3 wt % PE (i.e., PSS + PDADMA), both at 1.5 M KBr. Slowing the dynamics by varying the temperature from 20 to 5 °C has little effect on the *quasi*-CC, which remains in the terminal flow region with a reptation time at high frequencies. In contrast, the dynamics of the equivalent PSS solution appears significantly more temperature sensitive. As the temperature is lowered from 20 to 5 °C, the reptation time increases by 2 orders of magnitude, giving way to a rubbery plateau appearing at intermediate frequencies.

A time−temperature superposition was performed taking 20 °C as the reference temperature, as shown in Figure 7a. Only a horizontal shift factor, a_T, was applied. The dependence of the shift factor on the inverse of the absolute temperature (Figure 7b) was fitted using the Arrhenius equation.

$$\ln(a_T) = \frac{E_a}{R}\left(\frac{1}{T} - \frac{1}{T_{ref}}\right) \tag{3}$$

E_a is the activation energy, R is the gas constant, T is the absolute temperature of each testing condition and T_{ref} is the reference absolute temperature (293.15 K). The calculated activation energy for the *quasi*-CC and its equivalent PSS solution is 36 and 195 kJ mol^{-1}, respectively. The higher E_a and the appearance of a rubbery plateau in the case of the PSS solution implies stronger interactions between the PSS chains at this salt concentration, consistent with the report by Gulati and colleagues for a PSS of comparably high molecular weights (≥150 kg mol^{-1}).[48] As mentioned by these authors, the origin of these PSS−PSS interactions remains unclear. Nonetheless, our time−temperature superposition confirms their findings and suggests that the intra- and inter-molecular interactions among PSS chains in the *quasi*-CC are diluted by the presence of PDADMA (Figure 7a).

https://doi.org/10.1021/acs.macromol.5c02702
Macromolecules 2026, 59, 1383−1396

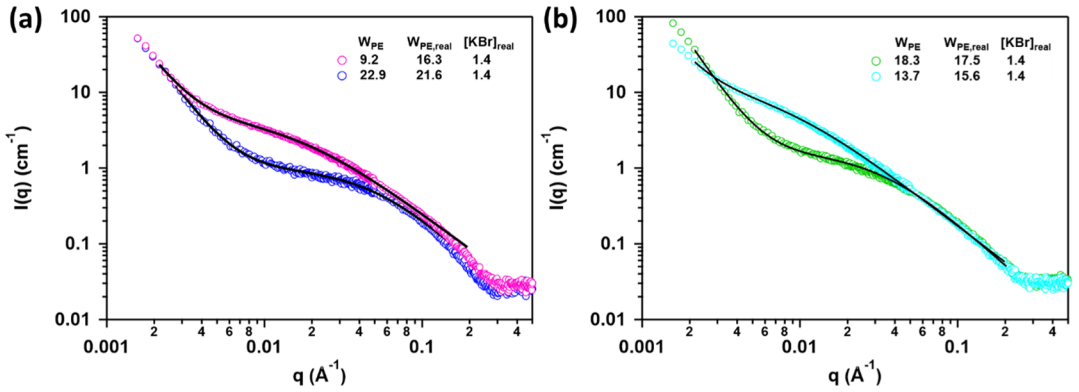

Figure 8. Scattering curves of two pairs of CC and their *quasi*-CCs formulated at 1.5 M KBr. Lines correspond to the fits with the scattering model. (a) CC prepared at 9.2 wt % and its *quasi*-CC prepared at 22.9 wt %, and (b) CC obtained at 13.7 wt % and its *quasi*-CC prepared at 18.3 wt %.

Structure of (*Quasi*)-Complex Coacervates

The macroscopic rheological behavior of CC and their corresponding *quasi*-CC are identical. For example, at 1.5 M KBr, the dynamic response of the CC obtained at W_{PE} = 9.2 wt % and the *quasi*-CC obtained at W_{PE} = 22.9 wt % are the same (Figures 4 and 5). Likewise, the CC obtained at W_{PE} = 13.7 wt % and the *quasi*-CC obtained at W_{PE} = 18.3 wt % have the same response. Nevertheless, these samples do not necessarily have the same composition (Figure 2b,c; the latter pair of CC and *quasi*-CC are quite close, with the CC on the binodal boundary and the *quasi*-CC just outside in the single-phase region). The similarity in the dynamic response and the differences in composition raise questions about the structure of these saline PE mixtures. Their structures were thus investigated by small-angle X-ray scattering (SAXS).

The scattering curves measured by SAXS contain structure functions related to both polymers. Without selective labeling, it is impossible to separate these contributions. Furthermore, considering the molar masses and polymer concentrations involved in the CC and *quasi*-CC, we are in the semidilute regime: each structure function holds information on the intra- (conformation) and inter-molecular correlations between chains segments. Getting information about their respective organization and/or their conformation (as well as the solvent quality) is not straightforward.

The scattering curves of liquid CC and *quasi*-CC prepared at 1.5 M KBr are shown in Figure S9 in the Supporting Information. PSS and PDADMA solutions at 1.5 M KBr were prepared and the scattering files were also recorded, as shown in Figure S10. The profiles of the saline liquid CC, *quasi*-CC, and PE solutions differ from that of classic salt-free PE solutions, which feature a typical correlation peak due to the strong repulsion of charged groups along the chains, preventing overlap among the correlation blobs.[49,50] The absence of a peak in all the PSS/PDADMA SAXS profiles (Figures S9 and S10) demonstrates a complete charge screening by the added KBr.[49,51] Data analysis was therefore performed considering a network of neutral polymers.

The scattering from a neutral polymer semidilute network or gel is usually described by an empirical correlation-length model (eq 4), capable of modeling both low and high q behaviors[39,52]

$$I(q) = \frac{a}{q^n} + \frac{b}{1 + (q\xi)^m} \quad (4)$$

The first term reflects scattering from large-scale inhomogeneities, which often lead to upturns at very low q. The second one describes the middle and high q regions. This Lorentzian-like function is associated with the semidilute polymer network of mesh size ξ (correlation length) and strands of fractal dimension m that reflects the nature of polymer−solvent interactions (m = 2 in θ solvent and 1.7 in good solvent). The polymer network scattering contribution tends to a plateau for $q \to 0$ and decays as q^{-m} at very high q. This latest domain, therefore linked to the form factor of individual chains, is only valid if the section of the chains can be neglected.

The scattering curves observed for CC and *quasi*-CC (Figure S9) showed the typical profile of semidilute polymer solutions or gels, as predicted by the model, with an upturn at low q, associated to large inhomogeneities, and a Lorentzian-like contribution related to the polymer network that changes with composition. Data of *quasi*-CC could be satisfactorily analyzed between 3×10^{-3} and 0.2 Å^{-1} (see Figure S9 and Table S3). The parameter m is close to 2 i.e. compatible with chains in θ solvents. As expected for polymers in semidilute regime, the correlation length is found to decrease gradually with increasing concentration. Despite this satisfactory agreement, several points need to be discussed.

(i) Concerning the origin of the scattered intensity, based on pure polymer solutions measurements (Figure S10b), we observe that scattering patterns appear almost flat for pure PDADMAC due a low contrast factor. Neglecting strong upturns at low q, we can anticipate that the PSS structure function dominates the scattering profile of PSS/PDADMAC samples below 0.1 Å^{-1}. This is analogous to contrast matching in small angle neutron scattering.[44] However, this is no longer the case at higher q.

(ii) We adjusted the profiles using a model that does not take into account the presence of two chain species with potential structural specificities. However, if the experimental decay up to 0.2 Å^{-1} is pretty well reproduced by the model, the high q power law variation (0.1 Å^{-1} < q < 0.2 Å^{-1}) could also reflect the local structural details of the two macromolecules (such as the length and the diameter of the Kuhn monomers) and result from a fortuitous combination of polymer structure functions rather than the chains' statistics alone. This may affect the fitted m parameters, and, to a lesser degree, the corresponding correlation lengths.

https://doi.org/10.1021/acs.macromol.5c02702
Macromolecules 2026, 59, 1383−1396

More sophisticated modeling is however complex to achieve without selective labeling.

The scattering intensity of the aforementioned CC at 1.5 M KBr are compared to their *quasi*-CC in Figure 8. The curves show the same characteristics, with a small upturn at low q and a Lorentzian-like contribution linked to the polymer network (with an apparent larger correlation length). They were analyzed with the same scattering model. The fitting parameters are summarized in Table S3. The values of the fractal dimension, m, are close to 1.6 and comparable to power law exponents previously reported for CC, characteristic of semidilute polymer solutions with a self-avoiding conformation.[49,53]

The correlations lengths of *quasi*-CC are therefore smaller than the ones of CC. This suggests that the single-phase samples outside the binodal are structurally different from the CC, even when they have a very similar composition (only the case for the pair in Figure 8b) and an identical dynamic response (the case for both pairs). This can be due to an inhomogeneous structure in the CC where the macro-ion pairs serve as transient physical cross-links, leading to polymer organization with a larger mesh size. On the contrary, in the absence of transient cross-links in the *quasi*-CC, the dynamics are mainly dominated by the entanglements rendering a more homogeneous nanostructure. Since rheological measurements provide bulk-averaged properties, they cannot directly reveal nanostructural differences. In contrast, SAXS data clearly demonstrates the structural distinctions between CC and *quasi*-CC, highlighting their structural differences despite similar bulk rheological properties.

SUMMARY AND CONCLUSIONS

Despite numerous works studying the effect of the added salt concentration on the complex coacervation, effects arising from changes in the total polymer concentration have been largely overlooked, leaving large areas of the phase diagram uncharted. The current work studied the composition, dynamics, and structure of viscoelastic liquids across the high-salt region of the phase diagram of high molecular weight PSS/PDADMA with KBr as added salt. The dynamic response of the materials was systematically probed along two types of pathways toward the single-phase region of the phase diagram. As expected, a typical salt pathway first results in swelling and eventually the suppression of phase separation at sufficiently high [KBr]. Along a PE pathway, i.e. at constant [KBr], the CC volume fraction increases toward the binodal boundary, accompanied with a slight increase in the water content, before the water content decreases beyond the binodal boundary. This is because of the lower gain in entropy along a PE pathway due to (i) the lower available volume of the SN for counterion release, and (ii) the increased total salt concentration because of the added counterions.

As expected, the swelling along a salt pathway is concomitant with significantly faster dynamics on observable time scales. The dynamics was also found to change as a function of the total W_{PE}, with faster dynamics toward the binodal and slower dynamics beyond. An important insight from this work is that this change in the dynamics of all the viscoelastic liquids on the same PE pathway occurs in a self-similar manner, allowing a time−PE superposition by applying a polymer concentration-dependent horizontal shift factor. The smallest shift factor, or the lowest viscosity, at each salt concentration corresponds to the sample at the binodal boundary, allowing precise quantitative prediction of the binodal limit based on the dynamic response of the system. Despite the self-similarity in the dynamics of PSS/PDADMA CC and their single-phase salty solutions, the shift factor a_P was found to have significantly different dependencies on the real polymer concentration, scaling with $W_{PE,real}^{11\pm1.5}$ and $W_{PE,real}^{4.1\pm0.5}$, respectively. While the single-phase materials behave as entangled solutions of neutral polymers in good solvent, the extreme exponent found in the case of the CC is due to the presence of a large number of stickers per chain and results in exponents exceeding the sticky reptation predictions. Such large exponents have been reported in CC obtained from poly(D,L-lysine hydrobromide) and poly(D,L-glutamic acid sodium salt), PSPMA/PTMAEMA, and PSS/PDADMA systems.[31−33] Due to the sparsity of studies focused on the effect of W_{PE} on the dynamics, further investigations are needed to verify if this strong dependence is specific to PSS/PDADMA. Our intuition is that this is not the case and that the CC exponent might be seen as a measure of the affinity of the macro-ion pairs for one another.

Moreover, the single-phase saline solutions of fully doped PSS/PDADMA mimic the viscoelastic behavior of their CC (up to the polymer solubility limit). These materials were called *quasi*-CC to highlight their distinction from both CC and saline solutions of an individual PE. It was further shown that the dynamics of all the liquid-like CC and *quasi*-CC prepared at different PE and salt concentrations is self-similar. A time−PE−salt superposition was introduced to unify the dynamics in the high-salt region of the phase diagram. A viscoelastic equivalent of a phase diagram combining the PE- and salt-concentration dependent shift factors as functions of PE concentrations was proposed.

Rheology and SAXS characterizations showed that both CC and *quasi*-CC behave as neutral polymers at elevated salt concentrations where electrostatic interactions are sufficiently screened. *Quasi*-CC are indeed mixtures of noninteracting PE solutions and hence essentially different from their CC counterparts. The CC were found to have a larger correlation length (i.e., larger mesh size) than their respective *quasi*-CC, which may arise from the ordered structure of CC due to the macro-ion pair associations. This is in good agreement with the differences in the mechanisms controlling their dynamics, i.e. reptation with many stickers per chain versus simple reptation in the case of CC and *quasi*-CC, respectively.

This work provides fresh insights into the dynamics and structure of viscoelastic liquids across the entire high-salt region of the phase diagram of oppositely charged PE. More adapted theoretical frameworks to describe the dynamics and structure of these materials remain of great interest.

ASSOCIATED CONTENT

Supporting Information

The Supporting Information is available free of charge at https://pubs.acs.org/doi/10.1021/acs.macromol.5c02702.

The Supporting Information file contains TGA verifications, the composition and phase behavior of the complex coacervates at different salt and polymer concentrations, the frequency sweeps at 1.3 and 1.75 M KBr, the Cole−Cole plots, the shift factors as a function of the total polyelectrolyte concentration, the frequency sweeps on PSS solution and *quasi*-CC at different

https://doi.org/10.1021/acs.macromol.5c02702
Macromolecules 2026, 59, 1383−1396

temperatures, as well as the SAXS data on CC, *quasi*-CC, and individual PSS and PDADMA solutions (PDF)

AUTHOR INFORMATION

Corresponding Author

Mehdi Vahdati − *CNRS, Institut Charles Sadron, Université de Strasbourg, Strasbourg 67200, France;* orcid.org/0000-0002-1823-998X; Email: mehdi.vahdati@ics-cnrs.unistra.fr

Authors

Jialin She − *CNRS, Institut Charles Sadron, Université de Strasbourg, Strasbourg 67200, France; Saint Gobain Recherche Paris, Aubervilliers 93300, France;* orcid.org/0009-0005-5994-9389

Axel Bourdette Kaya − *CNRS, Institut Charles Sadron, Université de Strasbourg, Strasbourg 67200, France*

Jérôme Combet − *CNRS, Institut Charles Sadron, Université de Strasbourg, Strasbourg 67200, France*

Matthew Tirrell − *Pritzker School of Molecular Engineering, University of Chicago, Chicago, Illinois 60637, United States; Center for Molecular Engineering and Materials Science Division, Argonne National Laboratory, Lemont, Illinois 60439, United States;* orcid.org/0000-0001-6185-119X

Francisco J. Cedano-Serrano − *Saint Gobain Recherche Paris, Aubervilliers 93300, France*

Fouzia Boulmedais − *CNRS, Institut Charles Sadron, Université de Strasbourg, Strasbourg 67200, France;* orcid.org/0000-0002-4934-9276

Complete contact information is available at: https://pubs.acs.org/10.1021/acs.macromol.5c02702

Author Contributions

The manuscript was written through the contributions of all authors, who have given their approval to the final version of the manuscript.

Notes

The authors declare no competing financial interest.

ACKNOWLEDGMENTS

For helpful discussions and feedback, the authors would like to thank Emmanuelle Gouillart, Marie Lamblet, Péroline Helbling, Marion Chenal, and Coralie Teulere from Saint-Gobain (FR), Pierre Schaaf (INSERM, University of Strasbourg), Alexander Semenov (ICS, CNRS), and Sina Ghiassinezhad (Université Catholique de Louvain). The authors acknowledge Mélanie Legros from the CARMAC platform (ICS, CNRS) for SEC analysis, as well as for access to the thermogravimetric apparatus and training of J.S. and A.B.K., and Guillaume Fleith from the DIFFERIX platform (ICS, CNRS) for conducting preliminary SAXS experiments. Saint-Gobain Research Paris and ANRT are acknowledged for the CIFRE fellowship (no. 2022-0982) granted to J.S. M.V. acknowledges financial support from ANR (ANR-22-CPJ2-0122-01). This work of the Interdisciplinary Institute HiFunMat, as part of the ITI 2021-2028 program of the University of Strasbourg, CNRS and Inserm, was supported by IdEx Unistra (ANR-10-IDEX-0002) and SFRI (STRAT'US project, ANR-20-SFRI-0012) under the framework of the French Investments for the Future Program.

REFERENCES

(1) Martin, N. Dynamic Synthetic Cells Based on Liquid−Liquid Phase Separation. *ChemBioChem* **2019**, *20* (20), 2553−2568.

(2) Sing, C. E.; Perry, S. L. Recent Progress in the Science of Complex Coacervation. *Soft Matter* **2020**, *16* (12), 2885−2914.

(3) Vahdati, M.; Hourdet, D.; Creton, C. Soft Underwater Adhesives Based on Weak Molecular Interactions. *Prog. Polym. Sci.* **2023**, *139*, 101649.

(4) Liu, Y.; Momani, B.; Winter, H. H.; Perry, S. L. Rheological Characterization of Liquid-to-Solid Transitions in Bulk Polyelectrolyte Complexes. *Soft Matter* **2017**, *13* (40), 7332−7340.

(5) Galland, P.; Iqbal, M. H.; Favier, D.; Legros, M.; Schaaf, P.; Boulmedais, F.; Vahdati, M. Tuning the Underwater Adhesiveness of Antibacterial Polysaccharides Complex Coacervates. *J. Colloid Interface Sci.* **2024**, *661*, 196−206.

(6) Cook, A. B.; Novosedlik, S.; van Hest, J. C. M. Complex Coacervate Materials as Artificial Cells. *Acc. Mater. Res.* **2023**, *4* (3), 287−298.

(7) Pace, G. T.; Le, M. L.; Clément, R. J.; Segalman, R. A. A Coacervate-Based Mixed-Conducting Binder for High-Power, High-Energy Batteries. *ACS Energy Lett.* **2023**, *8* (6), 2781−2788.

(8) Malekipirbazari, M.; Sadrameli, S. M.; Dorkoosh, F.; Sharifi, H. Synthetic and Physical Characterization of Phase Change Materials Microencapsulated by Complex Coacervation for Thermal Energy Storage Applications. *Int. J. Energy Res.* **2014**, *38* (11), 1492−1500.

(9) Ma, Y.; Wang, T.; Chang, X.; Liu, A.; Meng, X.; Liu, C.; Zhang, Y. Preparation of Isocyanate Microcapsules by Complex Coacervation and Its Application in Plywood. *J. Adhes.* **2024**, *100*, 890.

(10) Kim, E.; Jung, J. S.; Yoon, S. G.; Park, W. H. Eco-Friendly Silk Fibroin/Tannic Acid Coacervates for Humid and Underwater Wood Adhesives. *J. Colloid Interface Sci.* **2023**, *632*, 151−160.

(11) Chen, S.; Wang, Z.-G. Driving Force and Pathway in Polyelectrolyte Complex Coacervation. *Proc. Natl. Acad. Sci. U.S.A.* **2022**, *119* (36), No. e2209975119.

(12) Fu, J.; Schlenoff, J. B. Driving Forces for Oppositely Charged Polyion Association in Aqueous Solutions: Enthalpic, Entropic, but Not Electrostatic. *J. Am. Chem. Soc.* **2016**, *138* (3), 980−990.

(13) Vahdati, M.; Cedano-Serrano, F. J.; Creton, C.; Hourdet, D. Coacervate-Based Underwater Adhesives in Physiological Conditions. *ACS Appl. Polym. Mater.* **2020**, *2* (8), 3397−3410.

(14) Li, L.; Srivastava, S.; Andreev, M.; Marciel, A. B.; De Pablo, J. J.; Tirrell, M. V. Phase Behavior and Salt Partitioning in Polyelectrolyte Complex Coacervates. *Macromolecules* **2018**, *51* (8), 2988−2995.

(15) Chollakup, R.; Beck, J. B.; Dirnberger, K.; Tirrell, M.; Eisenbach, C. D. Polyelectrolyte Molecular Weight and Salt Effects on the Phase Behavior and Coacervation of Aqueous Solutions of Poly(Acrylic Acid) Sodium Salt and Poly(Allylamine) Hydrochloride. *Macromolecules* **2013**, *46* (6), 2376−2390.

(16) Spruijt, E.; Westphal, A. H.; Borst, J. W.; Cohen Stuart, M. A.; Van Der Gucht, J. Binodal Compositions of Polyelectrolyte Complexes. *Macromolecules* **2010**, *43* (15), 6476−6484.

(17) Digby, Z. A.; Yang, M.; Lteif, S.; Schlenoff, J. B. Salt Resistance as a Measure of the Strength of Polyelectrolyte Complexation. *Macromolecules* **2022**, *55* (3), 978−988.

(18) Neitzel, A. E.; Fang, Y. N.; Yu, B.; Rumyantsev, A. M.; De Pablo, J. J.; Tirrell, M. V. Polyelectrolyte Complex Coacervation across a Broad Range of Charge Densities. *Macromolecules* **2021**, *54* (14), 6878−6890.

(19) Kudlay, A.; Ermoshkin, A. V.; Olvera de la Cruz, M. Complexation of Oppositely Charged Polyelectrolytes: Effect of Ion Pair Formation. *Macromolecules* **2004**, *37* (24), 9231−9241.

(20) Schlenoff, J. B. Site-Specific Perspective on Interactions in Polyelectrolyte Complexes: Toward Quantitative Understanding. *J. Chem. Phys.* **2018**, *149* (16), 163314.

(21) Gucht, J. v. d.; Spruijt, E.; Lemmers, M.; Cohen Stuart, M. A. Polyelectrolyte Complexes: Bulk Phases and Colloidal Systems. *J. Colloid Interface Sci.* **2011**, *361* (2), 407−422.

(22) Wang, Q.; Schlenoff, J. B. The Polyelectrolyte Complex/Coacervate Continuum. *Macromolecules* **2014**, *47* (9), 3108−3116.

(23) Zhang, Z.; Chen, Q.; Colby, R. H. Dynamics of Associative Polymers. *Soft Matter* **2018**, *14* (16), 2961−2977.
(24) Spruijt, E.; Sprakel, J.; Lemmers, M.; Stuart, M. A. C.; Van Der Gucht, J. Relaxation Dynamics at Different Time Scales in Electrostatic Complexes: Time-Salt Superposition. *Phys. Rev. Lett.* **2010**, *105* (20), 208301.
(25) Hamad, F. G.; Chen, Q.; Colby, R. H. Linear Viscoelasticity and Swelling of Polyelectrolyte Complex Coacervates. *Macromolecules* **2018**, *51* (15), 5547−5555.
(26) Yang, M.; Shi, J.; Schlenoff, J. B. Control of Dynamics in Polyelectrolyte Complexes by Temperature and Salt. *Macromolecules* **2019**, *52* (5), 1930−1941.
(27) Manoj Lalwani, S.; Eneh, C. I.; Lutkenhaus, J. L. Emerging Trends in the Dynamics of Polyelectrolyte Complexes. *Phys. Chem. Chem. Phys.* **2020**, *22* (42), 24157−24177.
(28) Spruijt, E.; Cohen Stuart, M. A.; Van Der Gucht, J. Linear Viscoelasticity of Polyelectrolyte Complex Coacervates. *Macromolecules* **2013**, *46* (4), 1633−1641.
(29) Rubinstein, M.; Semenov, A. N. Dynamics of Entangled Solutions of Associating Polymers. *Macromolecules* **2001**, *34* (4), 1058−1068.
(30) Ali, S.; Prabhu, V. M. Relaxation Behavior by Time-Salt and Time-Temperature Superpositions of Polyelectrolyte Complexes from Coacervate to Precipitate. *Gels* **2018**, *4* (1), 11.
(31) Morin, F. J.; Puppo, M. L.; Laaser, J. E. Decoupling Salt- And Polymer-Dependent Dynamics in Polyelectrolyte Complex Coacervates via Salt Addition. *Soft Matter* **2021**, *17* (5), 1223−1231.
(32) Meng, X.; Du, Y.; Liu, Y.; Coughlin, E. B.; Perry, S. L.; Schiffman, J. D. Electrospinning Fibers from Oligomeric Complex Coacervates: No Chain Entanglements Needed. *Macromolecules* **2021**, *54* (11), 5033−5042.
(33) Landfield, H.; Wang, M. Diffusive Trends in Concentrated Oppositely-Charged Polyelectrolyte Solutions and Onset of Glassy Dynamics. *ACS Macro Lett.* **2024**, *13*, 1164−1170.
(34) Veis, A.; Bodor, E.; Mussell, S. Molecular Weight Fractionation and the Self-Suppression of Complex Coacervation. *Biopolymers* **1967**, *5* (1), 37−59.
(35) Sato, H.; Nakajima, A. Complex Coacervation in Sulfated Polyvinyl Alcohol-Aminoaeetalyzed Polyvinyl Alcohol System Ii. Formation of Coacervate Droplets. *Colloid Polym. Sci.* **1974**, *252*, 944−948.
(36) Dompé, M.; Vahdati, M.; Van Ligten, F.; Cedano-Serrano, F. J.; Hourdet, D.; Creton, C.; Zanetti, M.; Bracco, P.; Van Der Gucht, J.; Kodger, T.; Kamperman, M. Enhancement of the Adhesive Properties by Optimizing the Water Content in PNIPAM-Functionalized Complex Coacervates. *ACS Appl. Polym. Mater.* **2020**, *2* (4), 1722−1730.
(37) Syed, V. M. S.; Srivastava, S. Time-Ionic Strength Superposition: A Unified Description of Chain Relaxation Dynamics in Polyelectrolyte Complexes. *ACS Macro Lett.* **2020**, *9* (7), 1067−1073.
(38) Gulati, A.; Jacobs, M.; Lopez, C. G.; Dobrynin, A. V. Salt Effect on the Viscosity of Semidilute Polyelectrolyte Solutions: Sodium Polystyrenesulfonate. *Macromolecules* **2023**, *56* (5), 2183−2193.
(39) Colby, R. H. Structure and Linear Viscoelasticity of Flexible Polymer Solutions: Comparison of Polyelectrolyte and Neutral Polymer Solutions. *Rheol. Acta* **2010**, *49* (5), 425−442.
(40) Han, A.; Colby, R. H. Rheology of Entangled Polyelectrolyte Solutions. *Macromolecules* **2021**, *54* (3), 1375−1387.
(41) Dobrynin, A. V.; Jacobs, M. When Do Polyelectrolytes Entangle? *Macromolecules* **2021**, *54* (4), 1859−1869.
(42) Fujihara, I.; Tamura, K.; Murakami, S.; Fujishiro, R. Enthalpies of Dilution of Polymer Solutions. *Polym. J.* **1979**, *11* (2), 153−156.
(43) Dobrynin, A. V. Polyelectrolytes: On the Doorsteps of the Second Century. *Polymer* **2020**, *202*, 122714.
(44) Fang, Y. N.; Rumyantsev, A. M.; Neitzel, A. E.; Liang, H. I.; Heller, W. T.; Nealey, P. F.; Tirrell, M. V.; de Pablo, J. J. Scattering Evidence of Positional Charge Correlations in Polyelectrolyte Complexes. *Proc. Natl. Acad. Sci. U.S.A.* **2023**, *120*, No. e2302151120.
(45) Landfield, H.; Kalamaris, N.; Wang, M. Extreme Dependence of Dynamics on Concentration in Highly Crowded Polyelectrolyte Solutions. *Sci. Adv.* **2024**, *10*, No. eado4976.
(46) Parisi, D.; Ditillo, C. D.; Han, A.; Lindberg, S.; Hamersky, M. W.; Colby, R. H. Rheological Investigation on the Associative Properties of Poly(Vinyl Alcohol) Solutions. *J. Rheol.* **2022**, *66* (6), 1141−1150.
(47) Ricarte, R. G.; Shanbhag, S. A Tutorial Review of Linear Rheology for Polymer Chemists: Basics and Best Practices for Covalent Adaptable Networks. *Polym. Chem.* **2024**, *15* (9), 815−846.
(48) Gulati, A.; Han, A.; Colby, R. H.; Lopez, C. G. Rheological Properties of Concentrated Sodium in Aqueous Salt Solutions. *Macromolecules* **2024**, *57* (15), 7253−7262.
(49) Marciel, A. B.; Srivastava, S.; Tirrell, M. V. Structure and Rheology of Polyelectrolyte Complex Coacervates. *Soft Matter* **2018**, *14* (13), 2454−2464.
(50) Combet, J.; Lorchat, P.; Rawiso, M. Salt-Free Aqueous Solutions of Polyelectrolytes: Small Angle X-Ray and Neutron Scattering Characterization. *Eur. Phys. J.: Spec. Top.* **2012**, *213* (1), 243−265.
(51) Fares, H. M.; Ghoussoub, Y. E.; Delgado, J. D.; Fu, J.; Urban, V. S.; Schlenoff, J. B. Scattering Neutrons along the Polyelectrolyte Complex/Coacervate Continuum. *Macromolecules* **2018**, *51* (13), 4945−4955.
(52) Danielsen, S. P. O.; Beech, H. K.; Wang, S.; El-Zaatari, B. M.; Wang, X.; Sapir, L.; Ouchi, T.; Wang, Z.; Johnson, P. N.; Hu, Y.; Lundberg, D. J.; Stoychev, G.; Craig, S. L.; Johnson, J. A.; Kalow, J. A.; Olsen, B. D.; Rubinstein, M. Molecular Characterization of Polymer Networks. *Chem. Rev.* **2021**, *121* (8), 5042−5092.
(53) Spruijt, E.; Leermakers, F. A. M.; Fokkink, R.; Schweins, R.; Van Well, A. A.; Cohen Stuart, M. A.; Van Der Gucht, J. Structure and Dynamics of Polyelectrolyte Complex Coacervates Studied by Scattering of Neutrons, X-Rays, and Light. *Macromolecules* **2013**, *46* (11), 4596−4605.

https://doi.org/10.1021/acs.macromol.5c02702
Macromolecules 2026, 59, 1383−1396